

Self-consistent electronic structure method for broken-gap superlattices

T. Andlauer, T. Zibold, and P. Vogl*

Walter Schottky Institut, Technische Universität München, 85748 Garching, Germany

ABSTRACT

We present a novel charge self-consistent eight-band $\mathbf{k}\cdot\mathbf{p}$ envelope function method for the calculation of the electronic structure of type-II broken-gap heterostructures. Standard multiband $\mathbf{k}\cdot\mathbf{p}$ approaches fail to yield the correct occupation of electronic states in broken-gap heterostructures, because the strong hybridization of conduction band and valence band states is incompatible with the separate occupation of electron and hole states that is common to envelope function approaches. In our method, we occupy all included subbands with electrons according to the Fermi statistics and subsequently subtract a positive background ionic charge that guarantees charge neutrality. With this procedure, we have calculated local charge densities and subband dispersions of periodically n and p doped GaAs layers as well as effective band gaps of intrinsic InAs/GaSb superlattices.

Keywords: Electronic structure, type-II heterostructures, broken-gap

1. INTRODUCTION

The recent fabrication of high quality and high mobility antimonide heterostructures has revived the interest in this material class since their widely tunable electronic structure and optical properties offer many optoelectronic and electronic applications.¹⁻⁶ In combination with arsenide materials, antimonides can form type-II heterostructures with a broken gap. These types of heterostructures are particularly promising candidates for infrared lasers and infrared detectors. Unfortunately, mesoscopic quantum well systems with broken gaps are difficult to deal with in terms of standard theoretical band structure techniques such as effective mass theory. Once there is no gap, the chemical potential must be determined explicitly. However, standard effective mass theory tacitly assumes that electron and hole states are well separated from each other and can be occupied independently. Consequently, only few theoretical approaches have been developed so far to predict the electronic structure of nanostructures with broken gaps.⁶⁻⁹

In this paper, we present a novel electronic structure scheme for broken-gap materials that maintains the efficiency of a continuum approach yet does not depend on a separation into negatively charged electron and positively charged hole states. The key point in our approach is to remain in the electron framework throughout. The efficiency and accuracy of the method is illustrated by investigating GaAs doping superlattices. Furthermore, we predict subband energies of intrinsic InAs/GaSb superlattices as a function of the layer thickness in a regime where the superlattices exhibit a strong hybridization between electron-like and hole-like subband states near the Fermi energy.

The paper is organized as follows. In Sec. 2, we develop a charge self-consistent $\mathbf{k}\cdot\mathbf{p}$ envelope function method that is applicable to broken gap situations and compare it to the standard method. We assess this method in Sec. 3 by applying it to doping superlattices, where the spatial band gap can be tuned from positive to negative values simply by varying the doping concentrations. In Sec. 4, we apply our method to InAs/GaSb superlattices. Here, we focus on the critical regime where charge transfer between the individual layers takes place. Finally, the paper is summarized in Sec. 5.

*vogl@wsi.tum.de; phone +49-89-289-12750; fax +49-89-289-12737

2. MULTIBAND ENVELOPE FUNCTION METHOD

Broken-gap heterostructures are characterized by the lowest conduction band in one material layer to fall below the top valence band in an adjacent layer. This leads to a pronounced coupling of bands that needs to be taken into account properly if one wishes to calculate the electronic structure of such systems. Specifically, we consider multi-quantum well systems that consist of homogeneous layers laterally but may not be translation invariant along the growth axis z . Our approach is based on the eight-band $\mathbf{k}\cdot\mathbf{p}$ envelope function method.^{10–13} We represent the Hamiltonian in Fourier space with wave vectors \mathbf{k}_{\parallel} for the lateral directions and in terms of a discrete real space basis embracing N grid nodes with grid spacing Δ along the z -axis. The detailed Hamiltonian has been given in Ref. 14 and the method has been implemented in the freely available simulation package nextnano.¹⁵ Strain effects are incorporated into the Hamiltonian via linear band edge deformation potentials, and all material parameters have been taken from Ref. 16. The Schrödinger equation can be written schematically in the form

$$\sum_{\mu} \hat{\mathcal{H}}^{\nu\mu}(z, \mathbf{k}_{\parallel}) \Psi_i^{(\mu)}(z, \mathbf{k}_{\parallel}) = E_i(\mathbf{k}_{\parallel}) \Psi_i^{(\nu)}(z, \mathbf{k}_{\parallel}) \quad (\nu, \mu = 1..8, i = 1..8N). \quad (1)$$

The Hamiltonian $\hat{\mathcal{H}}$ has been patched up from the bulk $\mathbf{k}\cdot\mathbf{p}$ Hamiltonians $\hat{H}_{\mathbf{k}}$ of each constituent material by substituting $k_z \rightarrow -i\partial/\partial z$, which leads to the heterostructure Hamiltonian

$$\hat{\mathcal{H}}^{\nu\mu}(z, \mathbf{k}_{\parallel}) = \hat{H}_{-i\partial/\partial z, \mathbf{k}_{\parallel}}^{\nu\mu}(z) - e\phi(z) \delta_{\nu\mu}. \quad (2)$$

The indices ν, μ run over the two conduction and six valence bands. The eigenfunction $\Psi_i^{(\nu)}$ is the ν -th component of the i -th subband envelope function. The remaining wave vectors are restricted to the two-dimensional Brillouin zone Ω_{BZ} in the reciprocal \mathbf{k}_{\parallel} space. In order to take into account the spatial charge distribution, the general $8N$ dimensional Hamiltonian is augmented by the electrostatic potential $\phi(z)$ which obeys the Poisson equation

$$\Delta\phi(z) = -\frac{\rho_{\text{total}}(z)}{\varepsilon}. \quad (3)$$

Here, ε denotes the dielectric constant. Since the total charge density ρ_{total} depends on the eigenstates resulting from the Schrödinger equation, both differential equations have to be solved in a self-consistent manner. The total charge density can be written in the form

$$\rho_{\text{total}}(z) = \rho(z) - N_A^-(z) + N_D^+(z), \quad (4)$$

as it consists of the free carrier charge density $\rho(z)$ and the densities $N_A^-(z)$ and $N_D^+(z)$ of ionized acceptors and donors, respectively. Within the standard envelope function approach (EFA), the free carrier charge density $\rho = \rho_{\text{EFA}}$ is simply given by

$$\rho_{\text{EFA}}(z) = e[-n_{\text{EFA}}(z) + p_{\text{EFA}}(z)], \quad (5)$$

and is based on the assumption that the density of electrons in the conduction bands

$$n_{\text{EFA}}(z) = \sum_{i=6N+1}^{8N} \frac{1}{(2\pi)^2} \int_{\Omega_{BZ}} d^2\mathbf{k}_{\parallel} |\Psi_i(z, \mathbf{k}_{\parallel})|^2 f(E_i(\mathbf{k}_{\parallel})), \quad (6)$$

and holes in the valence bands

$$p_{\text{EFA}}(z) = \sum_{i=1}^{6N} \frac{1}{(2\pi)^2} \int_{\Omega_{BZ}} d^2\mathbf{k}_{\parallel} |\Psi_i(z, \mathbf{k}_{\parallel})|^2 [1 - f(E_i(\mathbf{k}_{\parallel}))]. \quad (7)$$

can be evaluated separately. The sums in these equations run over the energetically ordered subbands of the Hamiltonian and it is assumed that the first $6N$ subbands are valence band states and the remaining $2N$ subbands describe conduction bands. In addition, $f(E)$ is the Fermi function and the probability densities for a given subband i in an eight-band model are given by

$$|\Psi_i(z, \mathbf{k}_{\parallel})|^2 = \sum_{\nu=1}^8 |\Psi_i^{(\nu)}(z, \mathbf{k}_{\parallel})|^2. \quad (8)$$

If there is no global gap, however, it is not possible in general to decide if a specific eigenstate has to be occupied by an electron or by a hole since the conduction- and valence bands get coupled in a complicated way.

We have developed a novel method for the calculation of the free carrier charge density in multiband $\mathbf{k}\cdot\mathbf{p}$ models that accounts for the problem of overlapping bands and may be called full-band envelope function approach (FB-EFA).¹⁷ Rather than classifying the eigenstates into electron-like or hole-like, we occupy all eigenstates of the Hamiltonian $\widehat{\mathcal{H}}$ in Eq. (1) with electrons according to the Fermi-Dirac statistics. In addition, we subtract an appropriately calculated positive background ionic charge that guarantees charge neutrality. Thus, in this approach the charge density $\rho = \rho_{\text{FB-EFA}}$ is given by

$$\rho_{\text{FB-EFA}}(z) = e[-n_{\text{full-band}}(z) + \rho_{\text{bg}}(z)], \quad (9)$$

where $n_{\text{full-band}}(z)$ is the density of electrons from *all* occupied bands,

$$n_{\text{full-band}}(z) = \sum_{i=1}^{8N} \frac{1}{(2\pi)^2} \int_{\Omega_{BZ}} d^2\mathbf{k}_{\parallel} |\Psi_i(z, \mathbf{k}_{\parallel})|^2 f(E_i(\mathbf{k}_{\parallel})). \quad (10)$$

Note that the sum over i now runs over all $8N$ subbands of the Hamiltonian. In order to guarantee the electrical neutrality of the entire device, we must subtract the positive ionic core charge density,

$$\rho_{\text{bg}}(z) = 6N \frac{\Omega_{BZ}}{(2\pi)^2 \Delta}, \quad (11)$$

from the electron charge density. This density corresponds to the charge of $6N$ fully occupied valence subbands, and is assumed to be homogeneously distributed. The two-dimensional Brillouin zone area is given in terms of the lattice constant by $\Omega_{BZ} = 8\pi^2/a^2$. Since we consider a discrete z -space, the norm of any subband wave function is given by $\|\Psi_i^{(\nu)}\| = 1/\sqrt{\Delta}$. Correspondingly, the background charge density must be divided by the grid spacing Δ . This FB-EFA concept has been adapted from charge self-consistent tight-binding theory.¹⁸

Instead of integrating over the full Brillouin zone Ω_{BZ} , we can restrict the integration to the irreducible wedge Ω_{IW} of the Brillouin zone.^{19,20} For the cubic zinc blende quantum wells that we consider in this paper, this reduces the required numerical matrix diagonalizations by a factor of 8. Finally, there is another and even more important aspect that grossly reduces the computational effort. The sum in Eq. (10) runs over the entire two-dimensional Brillouin zone. Now, the calculation of all electronic states far from the zone center is not only time consuming, these states are actually poorly represented in an effective mass approach. Fortunately, states that deviate from the chemical potential μ by more than a few $k_B T$ are either empty and therefore do not contribute to the sum in Eq. (10) or are completely filled and can be taken into account by a corresponding adjustment of the background charge density. For antimonide based broken-gap systems, we find that the wave vectors of partially filled subband states lie within the inner 10% of the Brillouin zone Ω_{IW} . Only these \mathbf{k}_{\parallel} -states must be taken into account explicitly in Equation (10). This inner \mathbf{k}_{\parallel} space is mapped onto a discrete square wave vector lattice and the Schrödinger equation is solved for this set of discrete \mathbf{k}_{\parallel} -points. Finally, we have implemented a k -space integration scheme similar to Refs. 19, 21, 22 that linearly interpolates the probability densities and cubically interpolates the energy dispersion between the grid points in order to guarantee well converged results. More details have been described elsewhere.¹⁷

3. RESULTS: DOPING SUPERLATTICES

In order to assess the accuracy of the FB-EFA method, we consider a doping superlattice that consists of a single semiconducting material with periodic regions of n and p doping, respectively.²³ By varying the doping concentrations, we can achieve a continuous transition from a positive to a negative global spatial band gap. We will employ our FB-EFA [Eq. (9)] throughout this section, even in the case of weak doping where the material does show a positive energy gap and can be calculated in terms of the traditional EFA [Eq. (5)] for comparison. Concretely, we will analyze (001)-grown GaAs doping superlattices that consist of an alternating sequence of n and p doped layers with widths of 10 nm each. For the case of a positive band gap, we choose a doping concentration of $N_A = 2.6 \times 10^{19} \text{cm}^{-3}$ and $N_D = 5.2 \times 10^{19} \text{cm}^{-3}$. In the opposite limit of high doping that

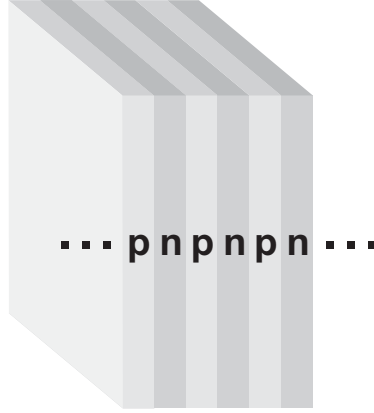


Figure 1. Sketch of GaAs doping superlattice considered in this paper. The structure consists of a periodic array of alternately n and p doped GaAs layers.

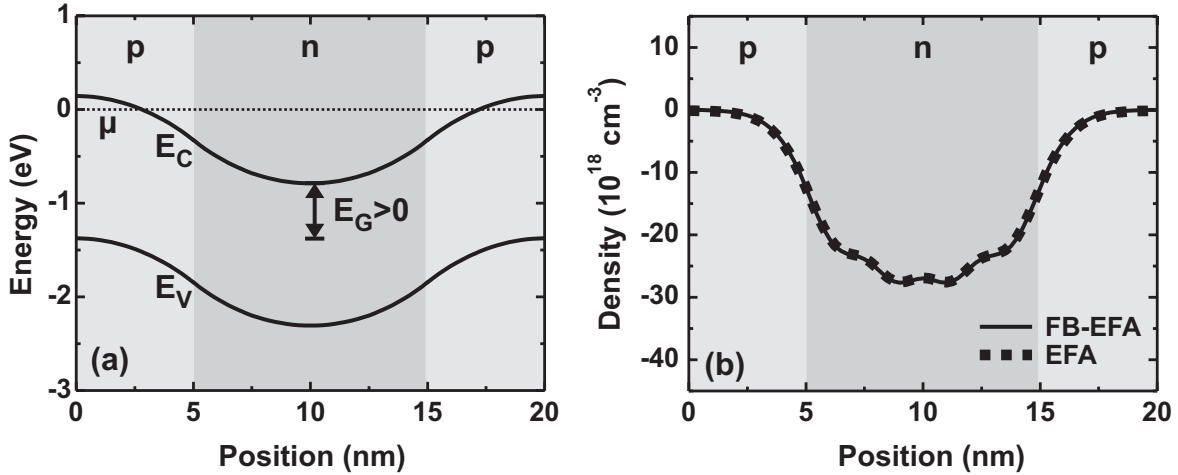


Figure 2. GaAs doping superlattice with p and n doping concentrations of $N_A = 2.6 \times 10^{19} \text{ cm}^{-3}$ and $N_D = 5.2 \times 10^{19} \text{ cm}^{-3}$, respectively. (a) The bulk band edges as a function of the position show a *positive* spatial band gap. (b) Calculated local free carrier charge densities ρ obtained with the present FB-EFA [Eq. (9)] (solid line) and the traditional EFA [Eq. (5)] (dotted line).

yields a broken gap situation, we set $N_A = N_D = 5.2 \times 10^{19} \text{ cm}^{-3}$. The temperature is set to $T = 4 \text{ K}$ in both cases. A sketch of the structure is shown in Fig. 1. We have calculated the charge self-consistent density and the band structure by iteratively solving the coupled system of the eight-band Schrödinger equation [Eq. (1)] and the Poisson equation [Eq. (3)] until self-consistency is reached.

We begin our discussion with the case of a globally positive band gap. Fig. 2 (a) shows the band edges of the lowest (bulk) conduction band $E_C - e\phi(z)$ and the top (bulk) valence band $E_V - e\phi(z)$ at the zone center including the electrostatic potential along the growth direction. All energies are given relative to the chemical potential μ that is indicated by the dotted black line. The minimum of the conduction band edge is larger in energy than the maximum of the valence band edge, so that the global band gap is positive and amounts to $E_G = 0.59 \text{ eV}$. In this situation, one can classify the eigenstates into electron-like and hole-like, simply according to their energetic position. Therefore, the charge density can be calculated with the present FB-EFA as well as with the standard EFA method. These two calculated free carrier charge densities are plotted in Fig. 2 (b) and are seen to be negative within the n-regions and zero otherwise. We note that the two densities coincide which

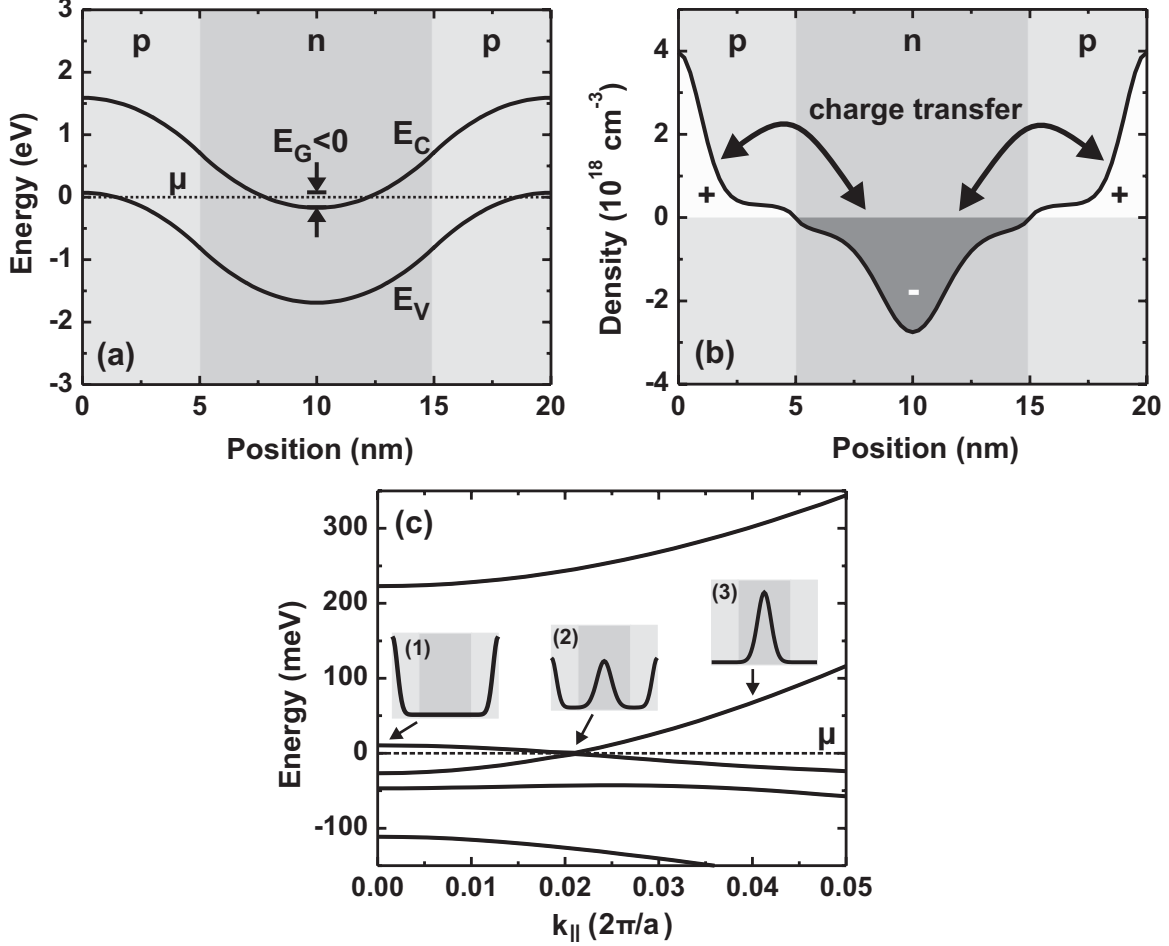


Figure 3. GaAs doping superlattice with p and n doping concentrations of $N_A = N_D = 5.2 \times 10^{19} \text{ cm}^{-3}$. (a) The bulk band edges as a function of the position show a *negative* spatial band gap. (b) Calculated local charge densities obtained with the present FB-EFA. The charge transfer between n and p doped layers is indicated in dark gray and white, respectively. (c) Subband dispersions as a function of k_{\parallel} in the lateral direction in units of $2\pi/a$, where a denotes the lattice constant of GaAs. The insets (1)-(3) show the probability density of the eigenstate of the lowest subband above the chemical potential μ at three different values of k_{\parallel} (0, 0.2, and 0.05).

confirms that FB-EFA yields the same results as EFA in situations where both methods are applicable.

We now turn to the situation of a globally negative band gap. By increasing the acceptor density, we enhance the band bending to a point where the lowest conduction band within the n region falls energetically below the top of the valence band within the p region. Fig. 3 (a) shows the band edges of the lowest conduction and highest valence band including the electrostatic potential, respectively. The global band gap is now negative and amounts to $E_G = -0.24 \text{ eV}$. In Fig. 3 (c), we show the energy dispersions of the subbands near the chemical potential μ , as a function of the in-plane wave vector along the [010] direction. This band structure has been calculated in terms of our FB-EFA method. It is interesting to examine the character of the subbands close to the chemical potential. At $k_{\parallel} = 0$, the lowest subband above μ can be seen from the inset (1) in Fig. 3 to be hole-like since it is almost completely localized within the p layers. For larger values of the wave vector, $|k_{\parallel}| \geq 0.04$ in units of $2\pi/a$, however, the character of this subband becomes electron-like, as can be deduced from inset (3) in Fig. 3 (c). For intermediate wave vectors, $|k_{\parallel}| = 0.02$, the band structure shows an anticrossing between the two subbands closest to μ that leads to a strong mixing of electron and hole states. Indeed, the probability

distribution shown in the inset (2) exhibits two distinct maxima that correspond to an almost equal localization of that state within the n and p layers. Obviously, these states cannot be classified as electron- or hole-like and effectively contribute to the electron as well as to the hole charge densities. Thus, it is not possible to simply occupy some subbands according to the Fermi-Dirac statistics of electrons and others with the statistics of holes as it is done in the standard EFA of Eq. (5).

In Fig. 3 (b), we show the free carrier charge density as calculated in terms of the FB-EFA method. We obtain a transfer of negative charge from the p -doped layers to the n -doped layers. This charge transfer can easily be explained by considering the character of the subbands as illustrated in Fig. 3 (c). The $\mathbf{k}_{\parallel} = 0$ eigenstate of the lowest subband above μ originates in the valence bands (see inset (1)). Since its energy is larger than the chemical potential, its occupation lacks electrons which in turn creates a positive charge contribution. Since the probability density of this state is localized within the p layers, we obtain a positive charge distribution in this layer. Analogous statements hold for all other wave vectors with $\mathbf{k}_{\parallel} < 0.02 \cdot 2\pi/a$ in this subband. Similarly, the zone center eigenstates of the highest subband below μ originate from the conduction band which leads to a negative charge distribution within the n layers. Altogether, we obtain a charge transfer of the order of 10^{18} cm^{-3} . Note that it would be difficult to accurately calculate such a small charge transfer in an atomistic approach that includes all electronic states in the Brillouin zone and therefore deals with charges of the order of 10^{23} cm^{-3} .

4. RESULTS: INAS/GASB SUPERLATTICES

In this section, we apply the FB-EFA to the electronic structure of InAs/GaSb type-II superlattices with a broken gap. A crucial property of such superlattices is the effective band gap E_G^{eff} , i.e. the energy difference between the lowest unoccupied (LU) and the highest occupied (HO) subband at $\mathbf{k}_{\parallel} = 0$. We consider intrinsic InAs/GaSb (001)-superlattices with InAs layer width w and a fixed GaSb layer width of 10 nm. The GaSb layer is assumed to be unstrained so that the InAs layers exhibit a slight tensile strain of 0.5%. In Fig. 4 (a), we sketch the corresponding bulk band edges of the zone center conduction band $E_C(z) - e\phi(z)$ (dotted line) and the heavy hole valence band $E_V(z) - e\phi(z)$ (solid line) that form a type-II broken-gap band alignment with a negative built-in band gap between the InAs and the GaSb layer. For small layer widths, carrier confinement raises the lowest electron subband above the highest hole subband,^{1,3} as indicated in the figure. We have calculated E_G^{eff} for superlattices with InAs layer widths w ranging from 4 to 30 nm at $T = 4 \text{ K}$ within the FB-EFA.

The results are plotted in Fig. 4 (b) and show that the effective band gap changes non-monotonously as a function of w . This behavior can be understood qualitatively by considering the two lowest electron-like (e_0, e_1) and two highest hole-like subbands (h_0, h_1) close to $\mathbf{k}_{\parallel} = 0$. With increasing InAs layer width w , the electron-like subbands decrease in energy due to the reduction in carrier confinement. By contrast, the hole subbands do not change their energetic position significantly, since the GaSb layer width is kept fixed. Thus, a change in w mostly changes the relative position of the electron-like states with respect to the hole-like ones. Consequently, the states that form the effective gap change abruptly whenever one of the e_i ($i = 0, 1$) subbands crosses a h_j ($j = 0, 1$) subband. This is indicated in Fig. 4 (b). For the smallest layer widths, the system behaves as a conventional semiconductor with $E(e_0) > E(h_0)$. The effective band gap decreases up to $w = 10 \text{ nm}$, where E_G^{eff} becomes zero. At this point, the subbands h_0 and e_0 switch their energetic positions so that E_G^{eff} now increases due to the reduction in confinement. At $w = 15 \text{ nm}$, e_0 falls below the second hole subband h_1 so that the effective gap is now formed by $E(h_0) - E(h_1)$. Since the energetic positions of these subbands only weakly depend on w , E_G^{eff} remains constant in this regime. In this manner, the trends in the effective gap can be explained. We would like to point out that for $w \geq 10 \text{ nm}$, a significant charge transfer between the InAs and GaSb layers occurs that leads to a band bending (indicated in Fig. 4 (a)) which shifts the lowest electron and hole subbands upwards and downwards, respectively. In addition, a charge self-consistent calculation is required to determine the chemical potential and therefore the HO and LU subbands. This demonstrates that a consistent theoretical model for broken-gap heterostructures is needed to predict realistic subband energies and effective band gaps.

5. SUMMARY

In summary, we have developed a novel charge self-consistent eight-band $\mathbf{k}\cdot\mathbf{p}$ envelope function method for the calculation of the electronic structure of type-II broken-gap heterostructures. Standard multiband $\mathbf{k}\cdot\mathbf{p}$

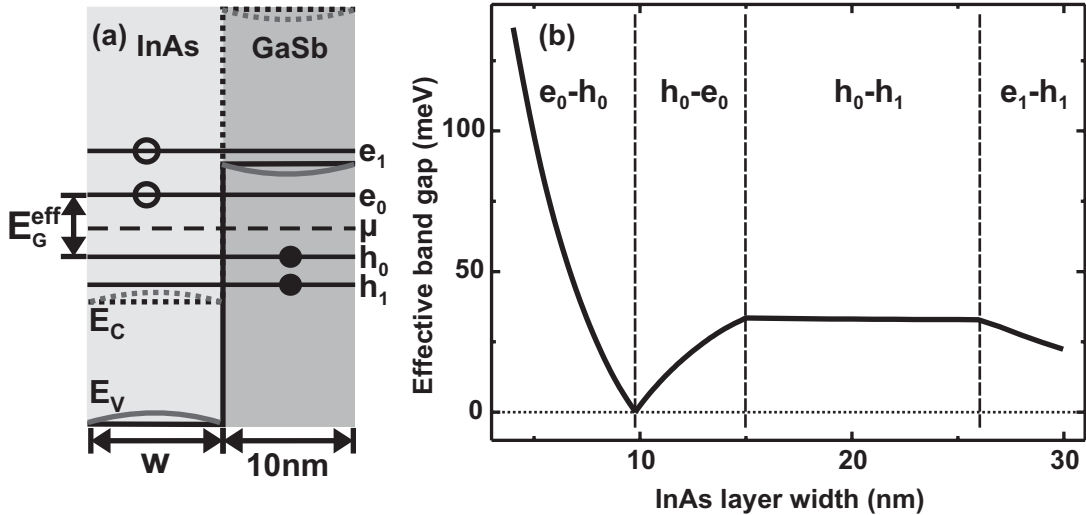


Figure 4. Calculated results for InAs/GaSb superlattices. (a) Qualitative sketch of the band edges in position space with zone center subband energies. The influence of charge transfer on the band structure is indicated schematically by the curved band edges (gray lines). (b) Calculated effective band gaps E_G^{eff} as a function of the InAs layer width w obtained by FB-EFA. Depending on w , the effective gap is formed by different subband states that are electron-like (e_i) or hole-like (h_j) at the Brillouin zone center.

approaches fail to yield the correct occupation of electronic states in broken-gap heterostructures, because the strong hybridization of conduction band and valence band states is incompatible with the separate occupation of electron and hole states. In the presently developed full-band envelope function approach (FB-EFA), all subbands get occupied with electrons according to the Fermi statistics. Subsequently, a positive background ionic charge is subtracted that guarantees charge neutrality. With this procedure, we have calculated local charge densities and subband dispersions of GaAs doping superlattices. We show that the FB-EFA method is equivalent to the standard EFA when applied to structures with a globally positive band gap. For negative band gaps, the FB-EFA correctly yields the charge transfer between the n and the p doped layers. In addition, we predict effective band gaps of intrinsic InAs/GaSb broken-gap superlattices as a function of the InAs layer width.

ACKNOWLEDGMENTS

The authors acknowledge support from the Deutsche Forschungsgemeinschaft (Grants No. SFB 631 and No. SPP 1285), the Austrian Science Fund FWF (SFB IRON), and the Nanosystems Initiative Munich (NIM).

REFERENCES

1. Dente, G. C. and Tilton, M. L., “Pseudopotential methods for superlattices: Applications to mid-infrared semiconductor lasers,” *J. Appl. Phys.* **86**, 1420–1429 (1999).
2. Poulter, A. J. L., Lakrimi, M., Nicholas, R. J., Mason, N. J., and Walker, P. J., “Intersubband transitions in InAs/GaSb semimetallic superlattices,” *Phys. Rev. B* **59**, 10785–10791 (1999).
3. Halvorsen, E., Galperin, Y., and Chao, K. A., “Optical transitions in broken gap heterostructures,” *Phys. Rev. B* **61**, 16743–16749 (2000).
4. Semenikhin, I., Zakharova, A., Nilsson, K., and Chao, K. A., “Effects of bulk inversion asymmetry and low interface symmetry on the optical properties of broken-gap heterostructures,” *Phys. Rev. B* **76**, 035335 (2007).
5. Xu, W., Wei, X. F., and Zhang, J., “Exchange-induced terahertz minigap in InAs/GaSb type II and broken-gap quantum wells,” *Appl. Phys. Lett.* **92**, 162108 (2008).

6. Liu, G. and Chuang, S.-L., "Modeling of Sb-based type-II quantum cascade lasers," *Phys. Rev. B* **65**, 165220 (2002).
7. Altarelli, M., "Electronic structure and semiconductor-semimetal transition in InAs-GaSb superlattices," *Phys. Rev. B* **28**, 842–845 (1983).
8. Xu, W., Folkes, P. A., and Gumps, G., "Self-consistent electronic subband structure of undoped InAs/GaSb-based type II and broken-gap quantum well systems," *J. Appl. Phys.* **102**, 033703 (2007).
9. Lapushkin, I., Zakharova, A., Yen, S. T., and Chao, K. A., "A self-consistent investigation of the semimetal-semiconductor transition in InAs/GaSb quantum wells under external electric fields," *J. Phys.: Condens. Matter* **16**, 4677–4684 (2004).
10. Luttinger, J. M. and Kohn, W., "Motion of electrons and holes in perturbed periodic fields," *Phys. Rev.* **97**, 869–883 (1955).
11. Bastard, G., "Superlattice band structure in the envelope-function approximation," *Phys. Rev. B* **24**, 5693–5697 (1981).
12. Burt, M. G., "Fundamentals of envelope function theory for electronic states and photonic modes in nanostructures," *J. Phys.: Condens. Matter* **11**, R53–R83 (1999).
13. Foreman, B. A., "Elimination of spurious solutions from eight-band k.p theory," *Phys. Rev. B* **56**, R12748–R12751 (1997).
14. Andlauer, T., Morschl, R., and Vogl, P., "Gauge-invariant discretization in multiband envelope function theory and g factors in nanowire dots," *Phys. Rev. B* **78**, 075317 (2008).
15. See <http://www.wsi.tum.de/nextnano> for obtaining the nextnano executables and related publications.
16. Vurgaftman, I., Meyer, J. R., and Ram-Mohan, L. R., "Band parameters for III-V compound semiconductors and their alloys," *J. Appl. Phys.* **89**, 5815–5875 (2001).
17. Andlauer, T. and Vogl, P. (to be published).
18. Majewski, J. A. and Vogl, P., "Simple model for structural properties and crystal stability of sp-bonded solids," *Phys. Rev. B* **35**, 9666–9682 (1987).
19. Gilat, G. and Raubenheimer, L. J., "Accurate numerical method for calculating frequency-distribution functions in solids," *Phys. Rev.* **144**, 390–395 (1966).
20. Cunningham, S. L., "Special points in the two-dimensional brillouin zone," *Phys. Rev. B* **10**, 4988–4994 (1974).
21. Cooke, J. F. and Wood, R. F., "Comparison of Brillouin-zone integration methods: Combined linear and quadratic interpolation," *Phys. Rev. B* **5**, 1276–1283 (1972).
22. Wiesenekker, G., te Velde, G., and Baerends, E. J., "Analytic quadratic integration over the two-dimensional Brillouin zone," *J. Phys. C: Solid State Phys.* **21**, 4263–4283 (1988).
23. Döhler, G. H., "Electron states in crystals with "nipi-Superstructure"," *Phys. Stat. Sol. (b)* **52**, 79–92 (1972).